Defluorination of Persistent Perfluoroalkyl Substances by Visible Light Under Ambient Conditions

Yuzo Arima, Yoshinori Okayasu, Yuki Nagai, Yoichi Kobayashi*

Department of Applied Chemistry, College of Life Sciences, Ritsumeikan University, 1-1-1 Nojihigashi, Kusatsu, Shiga 525-8577, Japan

*Corresponding author: ykobayas@fc.ritsumei.ac.jp

Perfluoroalkyl substances (PFASs) have been extensively utilized in various industries. However, their extremely high stability poses significant challenges, such as environmental persistence and waste treatment. Current PFAS decomposition approaches typically require harsh conditions. Thus, there is a pressing need to develop a new technique capable of decomposing them under mild conditions. Here, we showcase a method wherein perfluorooctanesulfonate, known as a "persistent chemical," and Nafion, a widely utilized sulfonated perfluoropolymer for ion-exchange membranes, undergo efficient decomposition into fluorine ions under ambient conditions via the irradiation of incoherent visible LED light onto semiconductor nanocrystals (NCs). This decomposition reaction is driven by cooperative mechanisms involving light-induced ligand displacements and Auger-induced electron injections via hydrated electrons and higher excited states. Our findings not only demonstrate the feasibility of efficiently breaking down various PFASs under mild conditions but also pave the way for advancing toward a sustainable fluorine-recycling society.

Introduction

Perfluoroalkyl substances (PFAS) exhibit excellent heat resistance, chemical resistance, insulating properties, and interfacial characteristics, rendering them indispensable in various industrial fields. However, the extremely strong carbon–fluorine (C–F) bond in these compounds leads to various environment-related challenges. For example, PFASs typically exhibit notable environmental persistence, and certain PFASs such as perfluorooctane

sulfonate (PFOS) and perfluorooctanoic acid (PFOA) are highly bioaccumulative. Moreover, waste treatment of fluorinated compounds is challenging because the hydrogen fluoride generated by the combustion of fluorinated compounds deteriorates incinerators.[1,2]

Several techniques have been reported to decompose PFAS into recyclable fluoride ions, including oxidation using strong oxidants such as peroxydisulfuric acid and ultraviolet-C (UVC) irradiation (wavelength below 260 nm) using a mercury lamp under high temperature and pressure.[3–13] Fluorine ions can be easily converted to calcium fluorides, which is a natural source of fluorine, and therefore, fluorine-recycling can be achieved. However, the use of mercury lamps as a light source is becoming less feasible owing to regulatory constraints imposed by the Minamata Convention on Mercury. A recent study demonstrates that perfluorooctanoic acid (PFOA) can be mineralized under strong basic conditions at 100 °C.[13] However, such mild conditions are not suitable for the decomposition of more stable PFASs, such as PFOS and perfluoroalkyl polymers. Despite the widespread use of fluoropolymers in diverse industrial applications, their recycling rate remains low, and many of them are subjected to landfill burial.[14] Therefore, it is necessary to develop a method to decompose extremely stable PFAS under mild conditions to address the multifaceted social issues linked with PFAS and to contribute to the realization of a sustainable fluorine-recycling society.

In this study, we demonstrate that PFOS and perfluoroalkyl polymers can be efficiently decomposed to fluorine ions in aqueous solutions at room temperature and atmospheric pressure through the irradiation of incoherent visible LED light onto cadmium sulfide (CdS) and copper-doped CdS (Cu-CdS) nanocrystals (NCs). While visible light energy is typically insufficient to break the strong C–F bonds, we overcome this limitation by stepwise two-photon absorption processes, in which photogenerated transient species absorb an additional photon to produce a higher excited state.[15–20] Semiconductor NCs exhibit high absorption coefficients and relatively long-lived excited states, facilitating the generation of multiple excited electrons. Under the circumstance, Auger recombination efficiently occurs, wherein the energy from the recombination of electron–hole pairs is transferred to another excited carrier to produce a higher excited state.[21,22] Typically, electrons in the higher state tend to relax to the lowest excited state

via nonradiative relaxation. However, a fraction of these electrons is either directly transferred to the PFAS when adsorbed onto the NC surface or is released into the medium, forming hydrated electrons. Hydrated electrons possess a reduction potential (−2.9 vs standard electron electrode (SHE)) exceeding that of metallic sodium,[23,24] and therefore can be used to decompose PFAS through reduction reactions. In colloidal NC systems, trapping of a photogenerated hole by hole scavengers likely extends the lifetime of the conduction band electron (Fig. 1), which facilitates the absorption of another photon to produce a negative trion (a three-carrier state composed of two electrons and a hole). Simultaneously, photoirradiation promotes the desorption of organic ligands from the NC surface, which in turn enhances the adsorption of PFAS onto the NC surface. Consequently, the efficient decomposition of PFAS occurs through cooperative multiphoton processes involving light-induced ligand displacements and Auger-induced electron injections via hydrated electrons and the higher excited states of NCs. This advanced decomposition technique can be applied to decompose other persistent chemicals under mild conditions, thus contributing to the realization of a sustainable fluorine-recycling society.

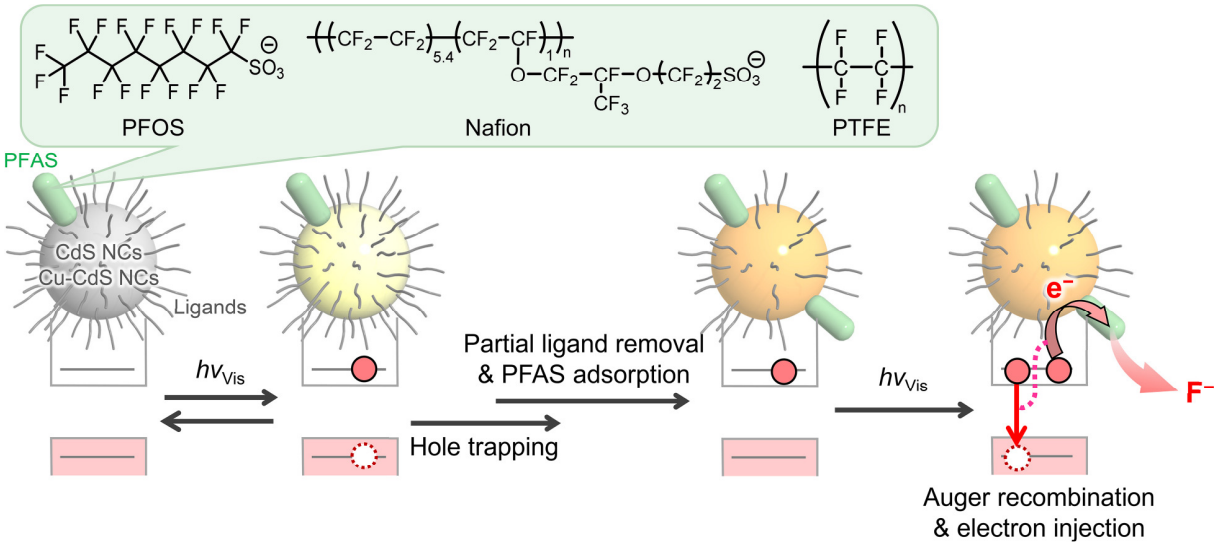

Fig. 1 Plausible reaction mechanism of visible-light-induced defluorination of PFAS by semiconductor NCs.

Results and discussions

Structural characterizations and steady-state optical properties

CdS and Cu-CdS NCs were synthesized in aqueous solutions using 3-mercaptopropionic acid (MPA), following a reported protocol.[25] X-ray diffraction (XRD) measurements showed that the crystal structures of CdS

and Cu-CdS NCs corresponded to zincblende structures, regardless of the amount of Cu (Supplementary Fig. S1). The average diameters of CdS NCs were estimated based on the excitonic absorption peak in the steady-state absorption spectra, [26] while those of Cu-doped CdS NCs were estimated by the peak width of XRD patterns. The atomic ratio of Cu per Cd ranged from 0–12%, as confirmed by X-ray fluorescence spectroscopy. Cu doping did not introduce XRD peaks related to impurities or optical absorption tails in the longer wavelength, indicating the absence of the Cu_xS domain. The synthesized aqueous solutions of MPA-capped CdS and Cu-CdS NCs exhibited absorption below 450–500 nm, depending on the size and composition (Supplementary Fig. S3). Cu doping slightly shifted the absorption spectra to a longer wavelength, probably because of the formation of midgap states dominated by Cu(3d) above the valence band.[27]

Transient absorption measurements to explore the generation of hydrated electrons

To investigate the photogenerated transient species, we conducted laser flash photolysis measurements using a 355-nm nanosecond laser pulse. As an example, the transient absorption spectra and dynamics of the aqueous solution of 12% Cu-doped CdS NCs are shown in Fig. 2 (results of CdS NC are shown in Supplementary Fig. S4). Immediately after the excitation, a broad positive transient absorption band was observed at 640 nm (Fig. 2a). The transient species decayed with a time constant of 0.90 μs (Fig. 2b). Moreover, the signal increased nonlinearly with increase in the excitation intensity (Fig. 2c). The spectral shape, lifetime, and nonlinear dependence indicated that the short-lived transient species originated from a hydrated electron generated by Auger processes.[28,29] Because the photon flux density was insufficient for a simultaneous two-photon process, the hydrated electron was produced by the stepwise two-photon process. The quantum yield for hydrated electron generation was estimated to be 1.5×10^{-2} when the excitation intensity was 4.0 mJ $pulse^{-1}$ (details can be found in Supplementary Note 1) The transient signal associated with the hydrated electron decayed faster (0.46 μs) upon the addition of PFOS to the solution (~6.2×10^{-4} M, Fig. 2d). This result shows that PFOS reacted with the generated hydrated electron.

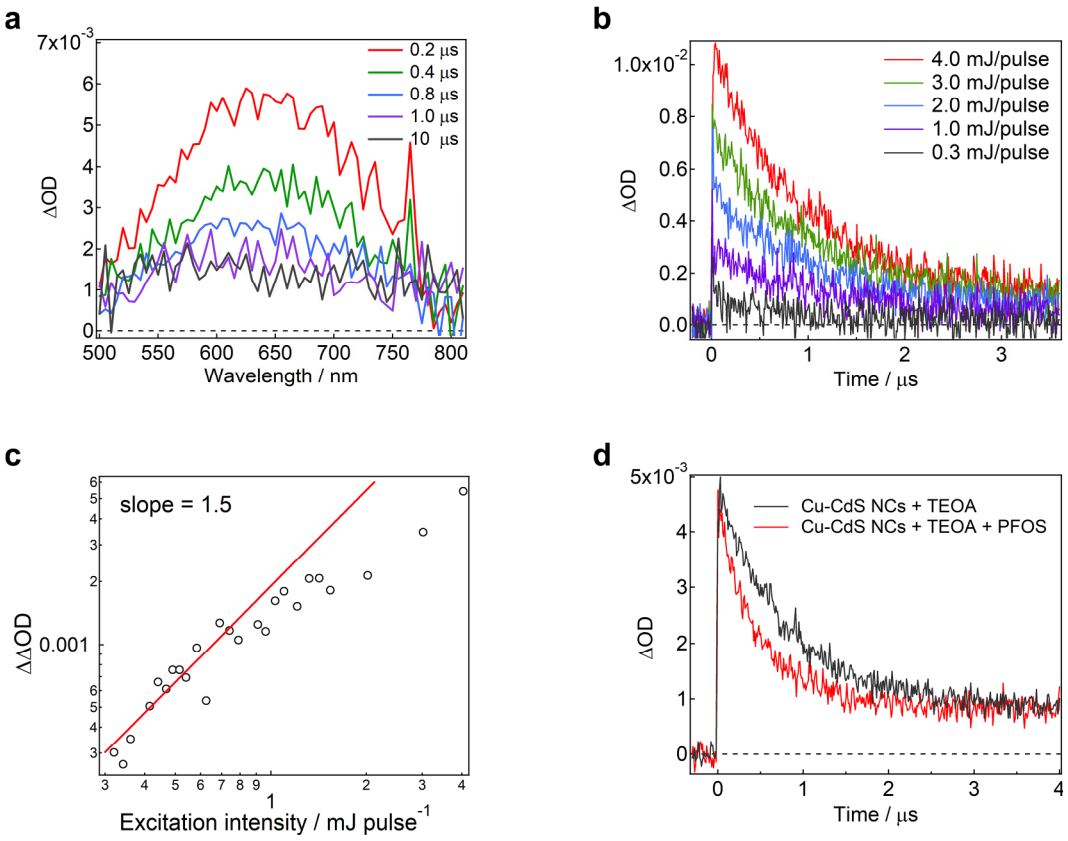

Fig. 2 | Generations of hydrated electrons by stepwise two-photon absorption processes. a, Representative transient absorption spectra of 12% Cu-CdS NCs excited with a 355-nm nanosecond laser pulse (4.0 mJ pulse^{-1}). **b**, Transient absorption dynamics at 700 nm under different excitation intensities. **c**, Amplitude of the submicrosecond decay component (ΔΔOD) as a function of excitation intensity. **d,** Reaction of the hydrated electron with PFOS in the presence of triethanolamine (TEOA).

Photocatalytic activities during PFOS decomposition

Solutions for photocatalytic reactions were prepared by adding CdS NCs, PFOS, and triethanolamine (TEOA, as a hole scavenger) to milli-Q water and N_2 bubbling (see Methods and Supplementary Table 1 for details). 405 nm LED light was irradiated into the solution to investigate the decomposition of PFOS (Supplementary Fig. 5). Full experimental conditions, along with the results of utilizing Cu-CdS NCs, are described in Methods and the supplementary information. The 19-fluorine nuclear magnetic resonance (^{19}F-NMR) spectrum of the reaction solution (deuterated water was used only for NMR measurements) before light irradiation originates from PFOS (Fig. 3a). After 405-nm light irradiation (830 mW cm^{-2}) for 24 h, only an intense sharp peak at −121 ppm was

observed, attributable to the fluorine ion. This observation shows that PFOS can be decomposed to fluorine ions by visible-light irradiation.

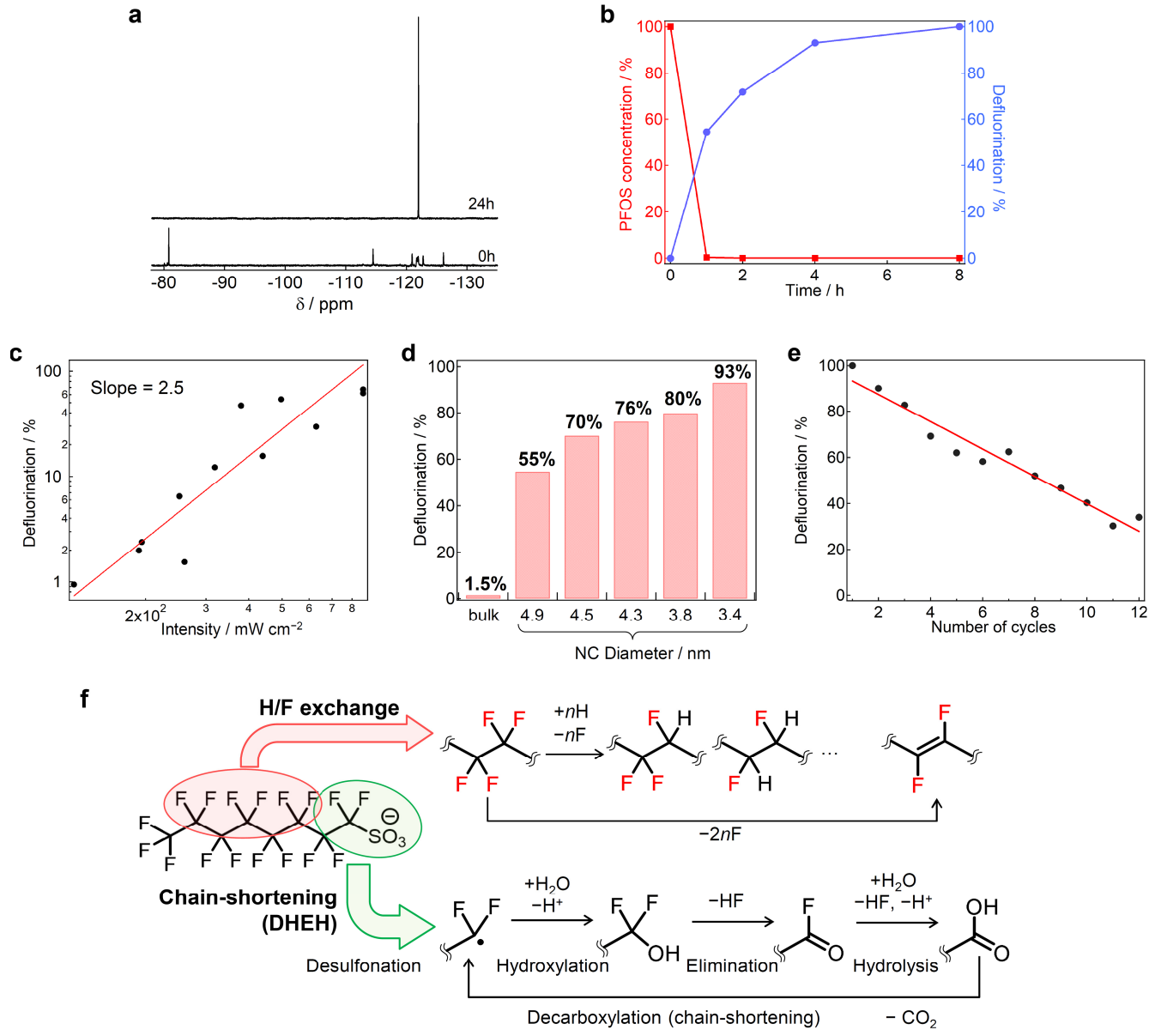

Fig. 3 | Photodecomposition of PFOS by irradiation of 405-nm LED light onto an aqueous solution containing PFOS, CdS NCs, and TEOA. a, ^{19}F-NMR spectra of the aqueous reaction solution before and after 405-nm light irradiation (830 mW cm^{-2}). **b,** Time profiles of PFOS concentration in the reaction solution and overall defluorination efficiency of the reaction solution. **c,** Dependence of the overall defluorination efficiency on irradiation power, and **d,** NC diameter. **e**, Repeated decomposition experiments using the same CdS NCs. One cycle includes 1) N_2 bubbling of the reaction solution for 30 min, 2) irradiation of 405-nm LED light for 12 h, 3)

centrifugation and removal of the supernatant, and 4) addition of 1.0 mL of the aqueous solution containing PFOS (1.2×10^{-6} mol) and TEOA (1.3×10^{-4} mol). The defluorination efficiency was measured for the solution subjected to centrifugation. Details of the experimental conditions can be found in the Methods section. **f**, Plausible decomposition mechanism of PFOS.

The overall defluorination efficiency (*overall* deF%, see equation (1) in the Methods section) increased with the increase in the irradiation period and reached almost the unity after 8 h (ranging from 90–100% depending on the experimental condition, Fig. 3b). The concentration of PFOS in the solution decreased with increase in the irradiation period and reached <0.1% after 8 h. The defluorination efficiency depends on the amounts of NCs and TEOA (Supplementary Fig. S8), and the optimized *overall* deF% were 55%, 70–80%, and 100% for 1-, 2-, and 8-h light irradiation, respectively. The quantum efficiency of C–F bond dissociations was determined to be 2.0×10^{-3} using the *overall* deF% after 1-h irradiation of 405-nm LED light (details can be found in Supplementary Note 2). Considering that the quantum efficiency for the generation of hydrated electrons was 1.5×10^{-2} under the nanosecond laser pulse excitation, the observed quantum efficiency for C–F bond dissociations using LED light appears remarkably high. This is probably due to the contribution of the direct electron transfer from higher excited states to the decomposition of PFOS in addition to the reaction with hydrated electrons. Similar photocatalytic behaviors were observed with Cu-CdS NCs (Supplementary Fig. 9).

The *overall* deF% after 4-h light irradiation exhibited a nonlinear dependence on the excitation intensity, even with LED light (Fig. 3c, with a slope of 2.5). This observation indicates multiphoton processes are involved in the PFOS decomposition. The reduction potential of the conduction band of CdS (−0.9 V vs. SHE)[30] is lower than that of PFOS (−1.3 V vs. SHE)[5] even taking the pH and quantum size effect into account (−1.19 V vs. SHE).[30,31] Moreover, the emission decay of CdS NCs was not affected at all by the presence of PFOS (Supplementary Fig. 10). These results strongly suggest that hydrated electrons and higher excited states generated by Auger recombination are involved in PFOS decomposition. The defluorination efficiency increased with decreasing NC

diameter (Fig. 3d), and the defluorination efficiency substantially decreased in commercial bulk CdS although the primary particle size estimated by the linewidth of X-ray diffractions was 7.4 nm. The efficient decomposition reaction in smaller NCs is consistent with the fact that Auger recombination is enhanced in a strong confinement regime and the rate of Auger recombination increases with smaller NC size in addition to the larger surface-to-volume ratio in smaller NCs.[21,22] Moreover, the slope of the power dependence in this study exceeded 2, whereas the experimentally observed slope of the power dependence of two-photon processes is typically below 2 owing to the involvement of other optical processes and reabsorption by photogenerated species. It suggests that another photochemical process is involved in PFOS decomposition, as discussed later.

The defluorination efficiency substantially decreased without hole scavengers (TEOA), owing to the photocorrosion of CdS NCs (Supplementary Fig. S11). In addition, the presence of molecular oxygen resulted in low defluorination efficiency (Supplementary Fig. S11). Several researchers have suggested that hydroxyl radicals generated by photogenerated holes are involved in PFAS decomposition.[32] Although we detected hydroxyl radicals with a hydroxyl radical probe (terephthalate anion) upon light irradiation, the generation of hydroxyl radicals was suppressed by the addition of TEOA (Supplementary Fig. S12). These results suggest that the photogenerated holes mainly lead to photocorrosion and do not contribute to the decomposition of PFOS in this system.

During the photocatalytic reactions, the NCs precipitated within tens of minutes of light irradiation, suggesting that the initial surface ligands of the NCs were desorbed or deteriorated by light irradiation. The XRD pattern and peak width of the precipitates indicated that the diameter of CdS NCs remained constant despite the photochemical reactions (Supplementary Fig. S13b). Fourier transform infrared (FTIR) spectra show that MPA was replaced with other organic molecules probably ascribed to TEOA and its photoproducts (Supplementary Fig. 13a). These results indicate that organic molecules on the surface of NCs dynamically change upon visible light, whereas NCs more or less retain their sizes. The precipitated CdS NCs could be reused to decompose PFOS over more than 12 cycles, although the *overall* deF% gradually decreased (Fig. 4e). Each cycle involved (1) N_2 bubbling of the reaction solution for 30 min, (2) irradiation of 405-nm LED light for 12 h, (3) centrifugation and decantation of the

supernatant, and (4) addition of 1.0 mL of the aqueous solution containing PFOS (1.2×10^{-6} mol) and TEOA (1.3×10^{-4} mol). The ratio of CdS NC and PFOS per cycle was 1:122.2, with each PFOS molecule containing 17 C–F bonds. The turnover number of C–F bond dissociation per CdS NC was calculated to be 1.72×10^3 from the line exploration. The concentration of cadmium (II) ions dissolved in the solution was 3 ppm after the 1st cycle, and varied between 6–46 ppm (the average was 13 ppm except for outliers) depending on the experimental conditions (Supplementary Fig. S14), which corresponds to 1–7% of the remained CdS NCs. The large deviation of the Cd concentration may be due to insufficient deoxygenation procedures because molecular oxygen promotes photocorrosion. The slight photocorrosion is consistent with the gradual decrease in the *overall* deF% by repeating the photocatalytic reactions.

Previous reports on PFOS decomposition by UVC light using a mercury lamp highlighted two potential mechanisms for PFOS decomposition: H/F exchange and chain-shortening (Fig. 3f).[3,6] The latter mechanism is known as decarboxylation (desulfonation as a first step)-hydroxylation-elimination-hydrolysis (DHEH) mechanism. Liquid chromatography-mass spectrometry (LC-MS) analyses before light irradiation suggested that the commercial linear PFOS used in this study contained several branched isomers, such as perfluoroheptanesulfonate (PFHpS, m/z = 449), perfluoroheptanesulfonate (PFHxS, m/z = 399), and a small amount of PFOA (m/z = 413, Supplementary Fig. S15-S27). After light irradiation for 1 h, the signals associated with PFOS substantially decreased, and multiple peaks originating from molecules with one or two F atoms of PFOS replaced with H atoms were observed (m/z = 481 and 463, Supplementary Fig. S28-S54). In addition, several peaks associated with molecules, where several even numbers of F atoms were abstracted and some of C–C bonds were converted to double or triple bonds, were observed (such as m/z = 461, 443, 425, 407, 405). These results suggested that the H/F exchange reaction occurred during the decomposition of PFOS. On the other hand, only products with fewer than three substituted hydrogen atoms were observed by H/F exchange, and the most defluorinated anion detected even after prolonged light irradiation was $C_8F_{10}H_3SO^{3-}$ (m/z = 369). Moreover, the signals associated with the anions generated by H/F exchange reactions decayed with increasing irradiation time. Considering the near-unity

defluorination efficiency in this system, another defluorination mechanism, i.e., the chain-shortening reaction likely occurred through visible-light irradiation. However, peaks derived from shorter-chain carboxylate anions, including trifluoroacetic acetate, were not observed even in the matrix-assisted laser desorption/ionization-time-of-flight mass spectrometry (MALDI-TOF MS) measurements of the solution after the reaction (Supplementary Fig. S102–S105). The absence of these small PFASs may indicate the efficient progression of DHEH reactions, resulting in the complete decomposition of PFOS to fluorine ions.

The adsorption of PFOS onto the surface of NCs is crucial for an efficient decomposition reaction. The decrease in the ^{19}F-NMR signals of PFOS dissolved in the aqueous solution by the addition of CdS NCs indicates that PFOS was promptly adsorbed onto the surface of NCs in the solution (Fig. 4a). LC-MS analyses revealed that 21% of PFOS were adsorbed on the surface of NCs 5 min after the addition of CdS NCs to the solution for photocatalytic reactions (Supplementary Fig. S106). Prior studies have shown that coordinated ligands are displaced under light irradiation, and the readsorption of displaced ligands requires more than several seconds.[33,34] The photoinduced ligand displacement was observed through proton-NMR (^{1}H-NMR) spectroscopy of the deuterated solution of MPA-capped CdS NCs (Fig. 4b). Broad peaks at 2.2–3.5 ppm before light irradiation were attributable to the MPA coordinated on the surface of NCs, while several sharp peaks were ascribed to weakly bound or free MPA. The sharp peaks associated with free MPA increased upon irradiation of 405-nm continuous-wave LED light (830 mW cm^{-2}) for 5 min. Moreover, the sharp peaks decreased again 1 h after light irradiation. These results indicated that MPA ligands were displaced by light irradiation, and the displaced MPA gradually readsorbed onto the NCs. This ligand displacement most probably facilitates the adsorption of PFOS onto the surface of NCs and accelerates the photodecomposition of PFOS. The timescale of the observed reaction was considerably slower than that reported previously, possibly because the extended duration of light irradiation promoted the persistence of displaced ligands.

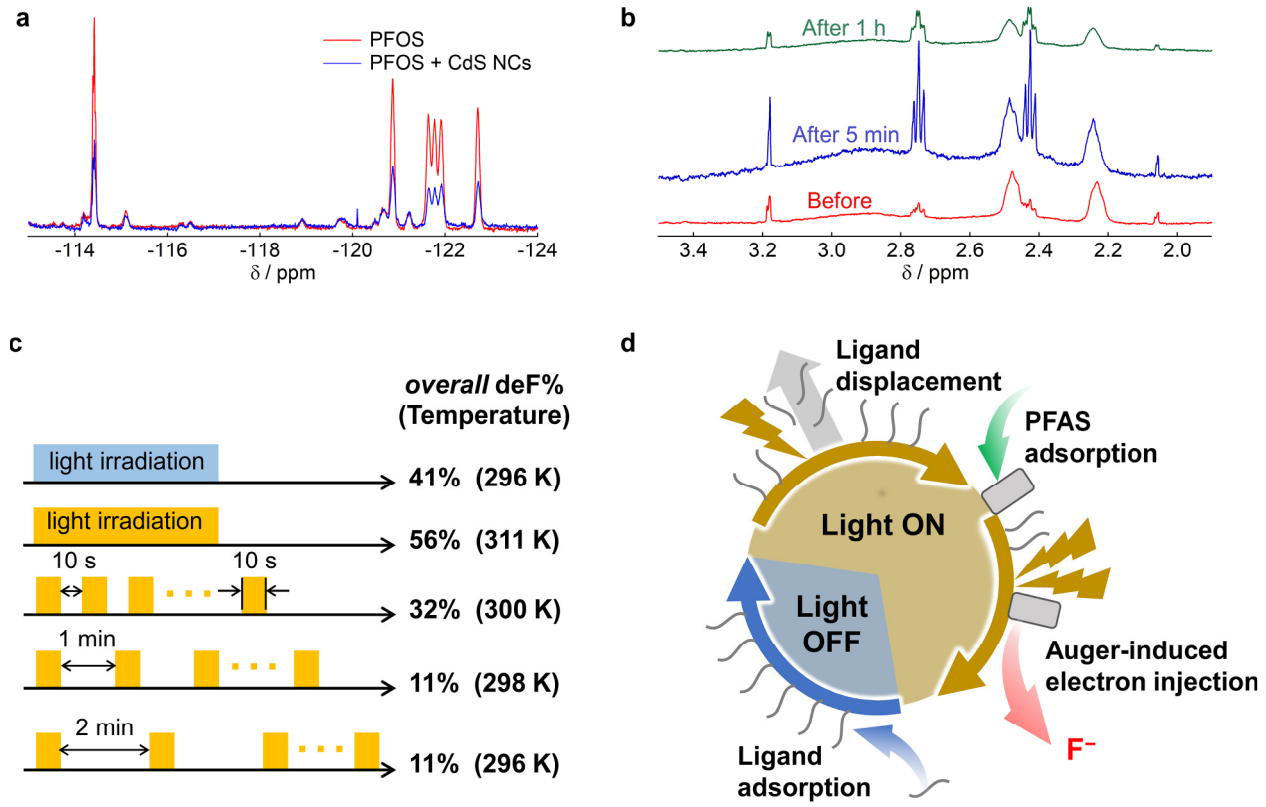

Fig. 4 | Effect of ligand desorption/adsorption reactions on PFAS decompositions. a, ^{19}F-NMR spectra of the aqueous solution of PFOS (1.2×10^{-3} M) before and after the addition of CdS NCs (2.7×10^{-4} M). **b**, ^{1}H-NMR spectra of CdS NCs before and after light irradiation (405 nm, 830 mW cm^{-2}) for 5 min. Broad peaks indicate MPA ligands coordinated to the surface of NCs, while sharp peaks correspond to free MPA. c, Schematics of light irradiation conditions, along with overall defluorination efficiency (*overall* deF%) and temperature of the reaction solution upon completion of light irradiation. **d**, Plausible mechanism underlying the relationship between ligand displacement and PFOS decomposition.

The reaction between PFOS and hydrated electrons, as well as higher excited states, should be completed within several microseconds. If the ligand displacement reaction plays a pivotal role in driving PFOS decomposition, the decomposition efficiency is expected to be affected by light irradiation conditions slower than seconds. To elucidate the relationship between ligand displacement on the NC surface and PFOS decomposition, we measured the *overall* deF% under different irradiation conditions. Specifically, the light was irradiated for 10 s and paused for specified intervals (10 s, 1 min, and 2 min, as illustrated in Fig. 4c). This cycle was repeated to achieve an

equivalent total irradiation duration as that of continuous irradiation for 1 h. Moreover, we monitored the solution temperature because it changes based on the duration of irradiation. Following continuous light irradiation for 1 h, the *overall* deF% was 56% and the solution temperature after the light irradiation was 311 K. The decrease in the solution temperature to 296 K under the same irradiation condition led to a decrease in the *overall* deF% to 41%. In contrast, 10-second irradiation intervals resulted in a decrease in the *overall* deF% to 32%, even though the solution temperature was 300 K. As the interval increased to 1 min, the *overall* deF% further decreased to 11% at 298 K, whereas the *overall* deF% maintained at 296 K with a 2-min interval. These observations indicate the involvement of another chemical reaction occurring on timescales of seconds to tens of seconds in PFOS decomposition. Moreover, the observed adsorption of displaced ligands, requiring several seconds to tens of seconds, and the slope of excitation dependence exceeding 2 highlight the significance of light-induced ligand desorption/adsorption reactions in PFOS decomposition. Once a ligand is desorbed, PFOS can coordinate with the NC surface, facilitating its efficient degradation. These results collectively suggest that the interplay between ligand desorption, PFOS adsorption, and nonlinear photoreaction processes plays a pivotal role in the efficient decomposition of PFOS under visible light (Fig. 4d).

Metal cadmium is expected to be generated upon light irradiation. Thus, its role in the defluorination reaction was experimentally studied. The generation of the metal cadmium on the NC surface was confirmed by a change in solution color from yellow to dark brown upon light irradiation.[35] The dark brown color persisted throughout the reaction and gradually faded over a day after the termination of light irradiation. This long lifetime of metal cadmium is inconsistent with the fact that the transient species contributing to the defluorination reaction are generated within a few seconds or tens of seconds. Notably, although the formation of metal cadmium was promoted by the addition of cadmium precursors ($CdCl_2$ or $Cd(CH_3COO)_2$), the *overall* deF% decreased (remaining nearly constant for $Cd(CH_3COO)_2$) with the addition of these precursors (Supplementary Fig. S107 and S108). These observations demonstrate that metal cadmium was not involved in the main pathways of defluorination reactions. Although sulfide ions and their byproducts may be potential photodegradation products of CdS, the reaction

efficiency did not improve even after the addition of sulfide ions (Supplementary Fig. S107). This result suggests that sulfur ions and their byproducts were not likely to be involved in the reaction.

This defluorination method can be applied to perfluorinated alkyl polymers such as Nafion (Fig. 1). Nafion is widely used as an ion-exchange membrane in electrolysis and batteries. For the powder form of Nafion, where the sulfonate groups are $-SO_2F$, the *overall* deF% under the same experimental condition with PFOS was at most 1.8% after irradiation for 24 h. When the same reaction was performed with Nafion dispersed in a water/ethanol mixture solution by saponification, where the sulfonate groups are $-SO_3^-$, the *overall* deF% dramatically increased to 81% over 24-h light irradiation. These results demonstrated that nonlinear photoreactions of semiconductor NCs can efficiently decompose perfluoroalkyl polymers, emphasizing the significance of proximity between the NCs and the substrate for the reaction. Furthermore, polytetrafluoroethylene (PTFE) powder can also be defluorinated, although the *overall* deF% was at most 5% after irradiation for 48 h. Images captured before and after the reactions demonstrated that the surface of the PTFE powder, which is strongly hydrophobic, became hydrophilic and the powder sank into the aqueous solution (Supplementary Fig. S112). In other words, PTFE can be defluorinated by visible LED light although the reaction efficiency was relatively low.

Conclusions

This research showcased the efficient defluorination of PFOS and Nafion using visible LED light irradiation onto semiconductor NCs at room temperature under atmospheric pressure. Because CdS is a typical compound semiconductor and nonlinear reactions are prevalent across various compositions, this demonstrated concept has the potential for broader applicability to other low-toxicity materials. The proposed methodology is promising for the effective decomposition of diverse perfluoroalkyl substances under gentle conditions, thereby significantly contributing towards the establishment of a sustainable fluorine-recycling society.

Methods

Materials

Cadmium chloride, anhydrous ($CdCl_2$), copper (II) chloride dihydrate ($CuCl_2 \cdot 2H_2O$), and sodium sulfide (Na_2S) were purchased from FUJIFILM Wako Pure Chemical Corp. (Osaka, Japan). MPA was purchased from Tokyo Chemical Industry Co. (Tokyo, Japan). The potassium salt of PFOS was purchased by Kanto Chemical Co. (Tokyo, Japan). Number average molecular weight (M_n) and weight average molecular weight (M_w) of Nafion (CAS No. 26654-97-7) were ~1.00×10^5 and ~1.83×10^5 ($M_w/M_n = 1.83$), respectively.

Synthesis of CdS and Cu-doped CdS NCs

MPA-capped CdS and Cu-doped CdS NCs were synthesized by following a previous study.[25] Specifically, 0.5 mmol of $CdCl_2$ was dissolved in 99 mL of deionized water. For Cu-doping, $CuCl_2 \cdot 2H_2O$ was also added to the solution. Then 1.25 mmol of MPA was added to the solution, and the pH of the solution was adjusted to 10–11 with 2.0 M NaOH aqueous solution. After N_2 bubbling for 30 min, 1.0 mL of 0.37 M Na_2S aqueous solution was quickly injected into the solution at 100°C and the solution was refluxed for 4 h to form the CdS NCs. The reaction time was varied to control the particle size. The obtained CdS NCs and Cu-doped CdS NCs were precipitated by methanol, the solution was centrifuged (8500 rpm, 5 min), and then the precipitate was dried in a vacuum.

Characterization

XRD patterns were recorded by an X-ray diffractometer (Rigaku Ultima IV). Organic functional groups on the surface of NCs were analyzed by an FTIR spectrometer (HORIBA FT-720 combined with an attenuated total reflection setup, resolution: 2 cm^{-1}) and JASCO FT/IR-6100. Steady-state absorption spectra were measured using UV-3600 (SHIMADZU), and the emission spectra were measured using FP-6500 (JASCO) and RF-6000 (SHIMADZU). X-ray fluorescence (XRF) measurements were performed using Supermini200 (Rigaku).

Ion chromatography was performed using an IC-8100EX (TOSOH, Tokyo, Japan) and using a TSKgel SuperIC-Anion HR column (4.6 × 150 mm, TOSOH, Tokyo, Japan) with a TSKgel guardcolumn SuperIC-A HS guard column (4.6 × 10 mm, TOSOH, Tokyo, Japan). The analysis was run using an eluent of 2.7 mM sodium carbonate and 2.2 mM sodium hydrogen carbonate using milli-Q water. A flow rate was 1.00 mL/min, giving the following

retention times: fluoride = 3.6-3.7 min. Milli-Q water was used as the calibration blank.

LC-MS measurements were performed using an LCMS-2050 (SHIMADZU, Kyoto, Japan) and using a Shim-pack XR-ODSII column (2.0 × 100 mm, SHIMADZU, Kyoto, Japan). A 20 mM aquated ammonium acetate: methanol gradient mobile phase at a flow rate of 0.25 mL/min was used for separation. Before ion chromatography and LC-MS measurements, liquid samples were filtered through a 0.22 μm nylon syringe filter (Membrane Solutions Ltd., Auburn, WA, USA).

Transient absorption measurements

Submicrosecond-to-microsecond transient absorption measurements shown in Fig. 2 were conducted using a TSP–2000 time-resolved spectrophotometer (Unisoku). The third harmonics (355 nm) of a 10 Hz Q–switched Nd:YAG laser (~5 ns pulse, Minilite II, Amplitude Japan) were used as the excitation light and the laser pulse was irradiated to the sample placed in a 10-mm quartz cuvette without a defocusing lens under nitrogen atmosphere. The results of nanosecond-to-microsecond transient absorption measurements shown in Supplementary Fig. 4 were obtained by the randomly-interleaved-pulse-train (RIPT) method.[36] A picosecond laser, PL2210A (EKSPLA, 1 kHz, 25 ps, 8.7 μJ/pulse for 355 nm), and a supercontinuum (SC) radiation source (SC-450, Fianium, 20 MHz, pulse width: 50–100 ps depending on the wavelength, 450–1000 nm), were employed as the pump–pulse and probe sources, respectively. The measurements were performed in an aqueous solution placed in a 2-mm quartz cell under argon condition with stirring at room temperature.

Photocatalytic hydrogen evolution and methanol oxidation

405-nm LED light (8332C, CCS Inc.) was collimated by a convex lens (f = 25 mm) and the light was irradiated to the solution in a 10-mm quartz cuvette (Supplementary Fig. 5). The spot area and the intensity were set to 1 cm^2 and 100-850 mW, respectively. The irradiation period was controlled by a homemade code using MATLAB.

All photocatalytic reaction conditions are summarized in Supplementary Table 1. In a typical photocatalytic

reaction setup, 1.0 mL of milli-Q water containing 0.8 mg of CdS NCs (equivalent to 1.0×10^{-8} mol for 3.4-nm CdS NCs), PFOS (0.65 mg, 1.2×10^{-6} mol), and TEOA (20 mg, 1.3×10^{-4} mol) to 1.0 mL of milli-Q water. Then the sample was mixed by sonication stirring for 10 min and nitrogen bubbling for 30 min in the 10-mm quartz cuvette. The decantation process for ion chromatography measurement was performed on centrifugation (15000 rpm, 5 min). The decomposition process of PFOS was monitored by ^{19}F-NMR spectroscopy, ion chromatography, and LC-MS measurements. Based on the concentration of fluorine ions released from the PFOS molecules into the aqueous solution, the *overall* deF% was calculated by the following equation,

$$overall\ \mathrm{deF\%} = \frac{[\mathrm{F^-}]}{n[\mathrm{PFAS}]_0} \times 100\ (\%) \qquad (1)$$

where $[\mathrm{F^-}]$, n, and $[\mathrm{PFAS}]_0$ are the concentration of fluorine ions, the number of C–F bonds per molecule (17 and 3460 for PFOS and Nafion, respectively), and the initial concentration of PFOS and the sulfonated polymer, respectively.

Data Availability. The data sets within the article and Supplementary Information of the current study are available from the authors upon reasonable request.

References

1. Ahrens, L. & Bundschuh, M. Fate and effects of poly- and perfluoroalkyl substances in the aquatic environment: A review. *Environ. Toxicol. Chem.* **33**, 1921–1929 (2014).
2. Martin, J. W., Mabury, S. A., Solomon, K. R. & Muir, D. C. G. Bioconcentration and tissue distribution of perfluorinated acids in rainbow trout (Oncorhynchus mykiss). *Environ. Toxicol. Chem.* **22**, 196–204 (2003).
3. Hori, H. *et al.* Decomposition of environmentally persistent perfluorooctanoic acid in water by photochemical approaches. *Environ. Sci. Technol.* **38**, 6118–6124 (2004).
4. Hori, H. *et al.* Efficient decomposition of environmentally persistent perfluorocarboxylic acids by use of persulfate as a photochemical oxidant. *Environ. Sci. Technol.* **39**, 2383–2388 (2005).
5. Park, H. *et al.* Reductive degradation of perfluoroalkyl compounds with aquated electrons generated from iodide photolysis at 254 nm. *Photochem. Photobiol. Sci.* **10**, 1945–1953 (2011).
6. Bentel, M. J. *et al.* Defluorination of Per- and Polyfluoroalkyl Substances (PFASs) with Hydrated Electrons: Structural Dependence and Implications to PFAS Remediation and Management. *Environ. Sci. Technol.* **53**, 3718–3728 (2019).
7. Dai, Y., Guo, X., Wang, S., Yin, L. & Hoffmann, M. R. Photochemical transformation of

perfluoroalkyl acid precursors in water using engineered nanomaterials. *Water Res.* **181**, (2020).
8. Qian, L., Kopinke, F. D. & Georgi, A. Photodegradation of Perfluorooctanesulfonic Acid on Fe-Zeolites in Water. *Environ. Sci. Technol.* **55**, 614–622 (2021).
9. Chen, Z. *et al.* Highly Efficient Hydrated Electron Utilization and Reductive Destruction of Perfluoroalkyl Substances Induced by Intermolecular Interaction. *Environ. Sci. Technol.* **55**, 3996–4006 (2021).
10. Cui, J., Gao, P. & Deng, Y. Destruction of Per- and Polyfluoroalkyl Substances (PFAS) with Advanced Reduction Processes (ARPs): A Critical Review. *Environ. Sci. Technol.* **54**, 3752–3766 (2020).
11. Duan, L. *et al.* Efficient Photocatalytic PFOA Degradation over Boron Nitride. *Environ. Sci. Technol. Lett* **7**, 613–619 (2020).
12. Chu, L. *et al.* Efficient decomposition of perfluorooctane sulfonate by hydrated electrons: Performance, mechanism, and carbon emission reduction. *J. Water Process Eng.* **49**, (2022).
13. Trang, B. *et al.* Low-temperature mineralization of perfluorocarboxylic acids. *Science* **377**, 839–845 (2022).
14. Améduri, B. & Hori, H. Recycling and the end of life assessment of fluoropolymers: recent developments, challenges and future trends. *Chem. Soc. Rev.* **52** 4208–4247 (2023).
15. Kobayashi, Y., Mutoh, K. & Abe, J. Stepwise two-photon absorption processes utilizing photochromic reactions. *J. Photochem. Photobiol. C* **34**, 2–28 (2018).
16. Glaser, F., Kerzig, C. & Wenger, O. S. Multi-Photon Excitation in Photoredox Catalysis: Concepts, Applications, Methods. *Angew. Chem. Int. Ed.* **59**, 10266–10284 (2020).
17. Schmalzbauer, M., Marcon, M. & König, B. Excited State Anions in Organic Transformations. *Ang. Chem. Int. Ed.* **60**, 6270–6292 (2021).
18. Kobayashi, Y. & Abe, J. Recent advances in low-power-threshold nonlinear photochromic materials. *Chem. Soc. Rev.* **51**, 2397–2415 (2022).
19. Parobek, D., Qiao, T. & Son, D. H. Energetic hot electrons from exciton-to-hot electron upconversion in Mn-doped semiconductor nanocrystals. *J. Chem. Phys.* **151**, (2019).
20. Widness, J. K. *et al.* CdS Quantum Dots as Potent Photoreductants for Organic Chemistry Enabled by Auger Processes. *J. Am. Chem. Soc.* **144**, 12229–12246 (2022).
21. Klimov, V. I. Optical Nonlinearities and Ultrafast Carrier Dynamics in Semiconductor Nanocrystals. *J. Phys. Chem. B* **104**, 6112–6123 (2000).
22. Kobayashi, Y., Nishimura, T., Yamaguchi, H. & Tamai, N. Effect of Surface Defects on Auger Recombination in Colloidal CdS Quantum Dots. *J. Phys. Chem. Lett.* **2**, 1051–1055 (2011).
23. Alfassl, Z., Bahnermann, D. & Henglein, A. Photochemistry of Colloidal Metal Sulfides. 3. Photoelectron Emission from CdS and CdS-ZnS Co-Colloids. *J. Phys. Chem.* **86**, 4656–4657 (1982).
24. Haase, M., Weller, H. & Henglein, A. Photochemistry of Colloidal Semiconductors. 26. Photoelectron Emission from CdS Particles and Related Chemical Effects. *J. Phys. Chem.* **92**, 4706–4712 (1988).
25. Han, Y. *et al.* Fast T-Type Photochromism of Colloidal Cu-Doped ZnS Nanocrystals. *J. Am. Chem. Soc.* **143**, 2239–2249 (2021).
26. Yu, W. W., Qu, L., Guo, W. & Peng, X. Experimental determination of the extinction coefficient of CdTe, CdSe, and CdS nanocrystals. *Chem. Mater.* **15**, 2854–2860 (2003).
27. Nelson, H. D. & Gamelin, D. R. Valence-Band Electronic Structures of Cu+-Doped ZnS, Alloyed Cu-In-Zn-S, and Ternary $CuInS_2$ Nanocrystals: A Unified Description of Photoluminescence across Compositions. *J. Phys. Chem. C* **122**, 18124–18133 (2018).
28. Haase, M., Weller, H. & Henglein, A. Photochemistry of Colloidal Semiconductors. 26. Photoelectron Emission from CdS Particles and Related Chemical Effects. *J. Phys. Chem.* **92**, 4706–4712 (1988).

29. Uchihara, T. *et al.* Nanosecond laser flash photolysis of thioglycerol-capped cadmium sulfide particles. *J. Photochem. Photobiol. A* **118**, 131–136 (1998).
30. Horst Kisch. *Semiconductor Photocatalysis Principles and Applications*. (Wiley, 2015).
31. Lippens, P. E. & Lannoo, M. Calculation of the band gap for small CdS and ZnS crystallites. *Phys. Rev. B* **39**, 10935–10942 (1989).
32. Hoffmann, M. R., Martin, S. T., Choi, W. & Bahnemann, D. W. Environmental Applications of Semiconductor Photocatalysis. *Chem. Rev.* **95**, 69–96 (1995).
33. Shulenberger, K. E., Keller, H. R., Pellows, L. M., Brown, N. L. & Dukovic, G. Photocharging of Colloidal CdS Nanocrystals. *J. Phys. Chem. C* **125**, 22650–22659 (2021).
34. Yoshioka, D. *et al.* Quasi-Reversible Photoinduced Displacement of Aromatic Ligands from Semiconductor Nanocrystals. *ACS Nano* **17**, 11309–11317 (2023).
35. GutiCrrez, M. & Henglein, A. Photochemistry of Colloidal Metal Sulfides. 4. Cathodic Dissolution of CdS and Excess Cd^{2+} Reduction. *Ber. Bunsenges. Phy. Chem.* **87**, 474–478 (1983).

Acknowledgments

This work was supported by JST, PRESTO Grant Numbers JPMJPR22N6, JSPS KAKENHI Grant Numbers JP21K05012. The authors express their gratitude to Dr. Tatsuo Nakagawa from UNISOKU Co., Ltd., for helping nanosecond to microsecond transient absorption measurements.

Author Contributions

Y.A. carried out whole experiment. Y.K. conceived and designed the whole experiment. Y.N. and Y.O. provided a technical guide. Y.K. wrote the manuscript. All authors participated in the discussion of the research.

Additional Information

Supplementary information accompanies this paper at http://www.xxx.

Competing financial interests

The Authors declare no Competing Financial or Non-Financial Interests.